Paper Number: **1500** *(replace with your paper number)*

Title: **Implementation of a Matrix Crack Spacing Parameter in a Continuum Damage Mechanics Finite Element Model**

Authors: Imran Hyder
Frank A. Leone
Brian P. Justusson
Joseph D. Schaefer
Andrew Bergan
Steven Wanthal

ABSTRACT

Continuum Damage Mechanics (CDM) based progressive damage and failure analysis (PDFA) methods have demonstrated success in a variety of finite element analysis (FEA) implementations. However, the technical maturity of CDM codes has not yet been proven for the full design space of composite materials in aerospace applications. CDM-based approaches represent the presence of damage by changing the local material stiffness definitions and without updating the original mesh or element integration schemes. Without discretely representing cracks and their paths through the mesh, damage in models with CDM-based materials is often distributed in a region of partially damaged elements ahead of stress concentrations. Having a series of discrete matrix cracks represented by a softened region may affect predictions of damage propagation and, thus, structural failure. This issue can be mitigated by restricting matrix damage development to discrete, fiber-aligned rows of elements; hence CDM-based matrix cracks can be implemented to be more representative of discrete matrix cracks. This paper evaluates the effect of restricting CDM matrix crack development to discrete, fiber-aligned rows where the spacing of these rows is controlled by a user-defined crack spacing parameter. Initially, the effect of incrementally increasing matrix crack spacing in a unidirectional center notch coupon is evaluated. Then, the lessons learned from the center notch specimen are applied to open-hole compression finite element models. Results are compared to test data, and the limitations, successes, and potential of the matrix crack spacing approach are discussed.

Imran Hyder, Boeing Research & Technology, North Charleston, South Carolina 29418
Frank A. Leone, NASA Langley Research Center, Hampton, Virginia 23681
Brian P. Justusson, Boeing Research & Technology, St. Louis, Missouri 63134
Joseph D. Schaefer, Boeing Research & Technology, St. Louis, Missouri 63134
Andrew Bergan, NASA Langley Research Center, Hampton, Virginia 23681
Steven Wanthal, Boeing Research & Technology, North Charleston, South Carolina 29418

INTRODUCTION

Computational progressive damage and failure analysis (PDFA) for finite element (FE) modeling is a key technology to enable timeline reduction for the design and certification of composite aerospace structures. However, existing PDFA methods are not mature enough to consistently provide accurate predictive capability for a continuously expanding design space [1]. Therefore, current industry design and certification approaches rely heavily on costly and time-intensive testing. It is therefore useful to evaluate PDFA accuracy through verification and validation to identify technology gaps for method improvement. These technology gaps can be addressed by experimental and theoretical studies to increase understanding of the material science governing damage development and progression, enhance conceptual formulations, improve method implementation, and identify requirements for FE model parameters.

A common validation test case for PDFA codes is the open-hole compression (OHC) specimen [2]. Although capturing stiffness and strength is necessary, focusing only on these two parameters potentially precludes validation that the underlying damage mechanisms are accurately captured. Damage development in OHC specimens is a function of both interlaminar and intralaminar damage events at the ply level, where intralaminar damage can be further broken down into matrix and fiber damage [3, 4, 5]. The damage events are discrete, sometimes competing mechanisms that eventually result in ultimate failure. PDFA methods must be able to predict correctly the onset, progression, and interaction of these discrete damage events.

Capturing discrete damage events can be difficult for certain continuum damage mechanics (CDM) approaches to PDFA [2], since intralaminar damage is represented by modifying the constitutive stiffness tensor in a continuum element rather than as a discrete fracture path and process. Without discretely representing cracks and their paths through the mesh, damage in models with CDM-based materials is often distributed in a region of damaged elements ahead of stress concentrations. Representing a series of discrete matrix cracks by a softened region may affect predictions of damage propagation and, thus, structural failure, especially for CDM methods derived to represent the presence of a single dominant matrix crack through the height of the element.

In order to make CDM damage more representative of discrete cracks, matrix damage can be restricted to separate, fiber-aligned rows of elements where matrix cracks are allowed to develop. The spacing of these rows of damageable elements can be controlled by a user-defined crack spacing parameter. The concept of crack spacing in a CDM approach has been explored previously in reference [6] for application to bolted joint specimens.

In this paper, the implementation of a matrix crack spacing approach is investigated. As an initial exercise, a center notch coupon loaded in Mode I and Mode II was used to compare the effects of varying the matrix crack spacing. Lessons learned from this initial exercise were then applied to the prediction of damage development in OHC specimens. The CDM PDFA method was implemented with two approaches: a conventional approach, where both matrix and fiber damage were enabled throughout the area of interest, and with a modified approach, where a minimum matrix crack spacing distance was enforced. Results from both implementations were compared against experimental stress-strain curves and X-ray computed tomography (CT) scans to highlight the differences in predictions in terms of damage size and location. The

PDFA method that was used in this study is CompDam. CompDam is a CDM-based research code developed at NASA Langley Research Center, implemented as an Abaqus user-defined material subroutine (VUMAT) [7, 8]. This study used the IM7/8552 material system, and input property values were obtained from [9].

CENTER NOTCH TENSION AND SHEAR MATRIX CRACK SPACING EXERCISE

The objectives of the Center Notch Tension (CNT) and Center Notch Shear (CNS) analyses included obtaining a qualitative understanding of the effects of enforcing a minimum matrix crack spacing in models with CDM materials and assessing whether a recommendation could be made regarding the minimum number of non-damageable elements that should be kept between adjacent matrix cracks. This was accomplished by evaluating the stress fields ahead of a region of cracks with varying matrix crack spacing. Allowing damage to exist everywhere is herein referred to as a damage fully enabled (DFE) approach, whereas restricting damage to pre-identified fiber-aligned rows of elements is herein referred to as a matrix crack spacing (MCS) approach.

The geometry, mesh, section assignments, step definition, and boundary conditions used in the analysis models all follow the procedures outlined in [10] and [11]. Schematics of these models are shown in Figures 1 and 2. Plane stress elements with reduced integration (CPS4R) were used, where the typical element length ahead of the notch tip was $L_e = 0.25$ mm. Unlike the CNT and CNS models from [10] and [11], multiple pre-damaged CDM cracks were defined in the model for different values of the MCS parameter. The MCS values that were assessed were 0, 1, 3, and 5. The MCS parameter corresponds to the number of undamaged elements between adjacent potential matrix cracks, where an MCS value of 0 is the same as the DFE approach. In all cases, the pre-cracked region had a height of 23 elements. The MCS value of 0 then yielded a 23-element-wide blunt notch. Results for both Mode I (CNT) and Mode II (CNS) loading were extracted at the same point in the load history for each analysis, before the initiation of any additional damage.

The results from the CNT and CNS analyses are shown in Figure 3 and Figure 4, respectively. In the figures, contour plots of the dominate stress component (σ_{22} for Mode I and σ_{12} for Mode II) are shown for each value of MCS. In addition, the stress at element integration points immediately ahead of the crack tips is plotted as a function of the height of the cracked region. These plots show that the stresses ahead of the crack tips for MCS values of 0 and 1 are similar for both Mode I and II loading conditions, where there are no discernible peaks corresponding to the individual crack tips. Therefore, it is concluded that MCS = 1 is not sufficient to represent the discrete nature of neighboring matrix cracks. For MCS values of 3 and 5, a clear different trend can be observed in that there are discernible peaks corresponding to each crack tip in both the normal and shear stress distributions. Qualitatively, it can be concluded that an MCS ≥ 3 is required to adequately represent discrete stress concentrations ahead of neighboring matrix cracks. This exercise provides a lower limit for MCS. An upper limit of an acceptable MCS value cannot be concluded from this exercise. The upper limit for MCS is related to the matrix crack spacing at saturation for the subject material. The upper limit to MCS may also depend on whether capturing crack saturation is necessary for a given analysis.

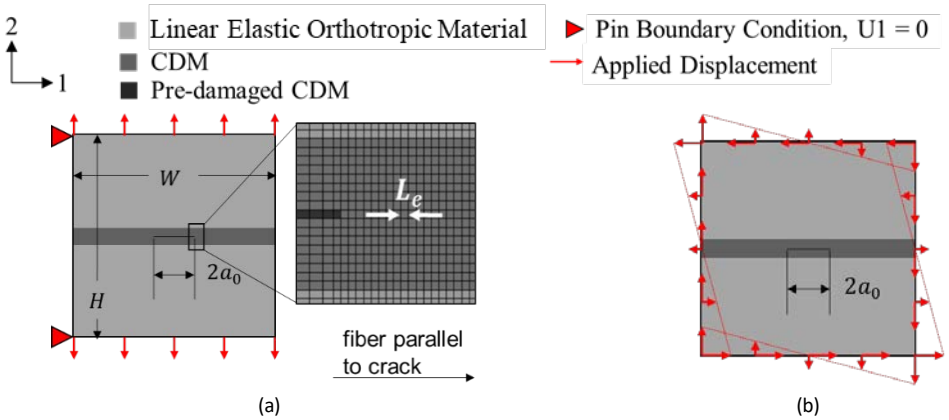

Figure 1. Boundary conditions, section assignments, and geometry for (a) CNT and (b) CNS. *W*, *H*, and a_0 are 127 mm, 127 mm, and 12.7 mm, respectively.

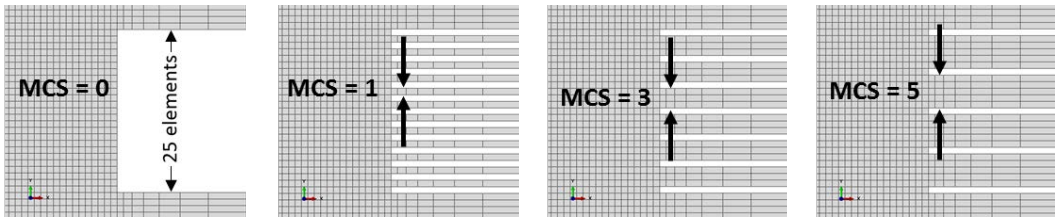

Figure 2. CNT/CNS models with MCS values of (a) 0, (b) 1, (c) 3, and (d) 5. Elements in the cracks were pre-failed by defining the matrix damage variable via initial conditions to represent a traction-free state.

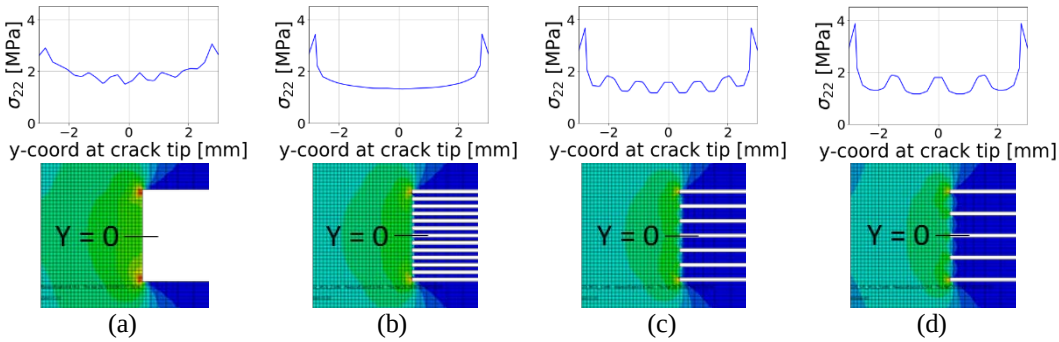

Figure 3. Mode I crack tip normal stress (σ_{22}) versus crack region height plots with their corresponding stress contour plots for MCS values of (a) 0, (b) 1, (c) 3, and (d) 5.

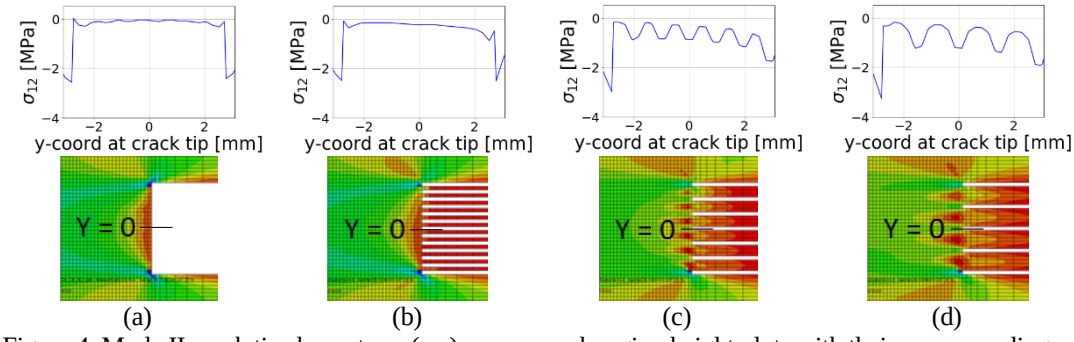

Figure 4. Mode II crack tip shear stress (σ_{12}) versus crack region height plots with their corresponding stress contours plots for MCS values of (a) 0, (b) 1, (c) 3, and (d) 5.

OPEN-HOLE COMPRESSION

Experimental Procedure

Compression testing was performed on open-hole specimens with three laminate configurations, referred to herein as the Soft, Quasi, and Delam laminates, where the layups are shown in Table I. These layups were selected to assess model performance for predicting laminate-dependent progression of critical damage modes and interactions, and to assess the effects of damage development on laminate stiffness and strength.

The Soft laminate was expected to have a highly nonlinear pre-peak load-displacement response due to the inclusion of 80% ±45° plies. The Quasi laminate was similar to skin layups typically used by industry. The Delam laminate was designed to develop significant amounts of delamination. The specimens were sized and tested according to American Society for Testing and Materials (ASTM) D6484 Procedure A [12]. The specimen dimensions were 38.1 mm by 177.8 mm, and included a 3.175 mm radius hole. Ply thickness was 0.183 mm. The tests were conducted at room temperature, and the specimens were loaded at a rate of 0.6 mm/min on a 245 kN load frame. Digital Image Correlation (DIC) was used for obtaining displacement and strain fields. A 50.8 mm virtual extensometer, centered at the hole and aligned with the loading axis, was used to obtain displacement and strains for comparison against finite element analysis (FEA). Stress was obtained by dividing the applied load by the cross sectional area. Five specimens were tested for each laminate. The first three specimens were loaded until failure, whereas the fourth and fifth specimens were loaded to 75% and 90% of the average failure load of the first three replicates. The ply-by-ply damage state was characterized using post-test X-ray CT imaging. The damage observed in the X-ray CT scans of the specimens loaded to 75% and 90% of peak load was plotted with the load versus displacement data to compare experimental observations of damage with model predictions. Specimens were not reloaded. Data at each load threshold is from a different specimen loaded to that threshold; therefore, the actual results may be different from scan to scan and the damage modes should be considered representative of the observable failure process. Detailed explanation on the experimental procedure can be found in [13].

Table I. OHC Laminate Definitions

Name	Stacking Sequence
Soft	$[+45/-45/0/+45/-45/90/+45/-45/+45/-45]_S$
Quasi	$[+45/0/-45/90/+45/0/-45/90/+45/0/-45/90]_S$
Delam	$[(+45/-45/0_2)_3]_S$

Analysis Procedure

The model geometry, boundary conditions, and general section property assignment definitions are illustrated in Figure 5. The models were assigned elastic material properties and CDM material properties to non-damageable and damageable sections, respectively. The damageable region (i.e., the CDM region) was chosen such that damage development occurred well within this region and did not reach the non-

damageable material. The length of the damageable region was approximately 55 mm. Nodal displacements were obtained by two nodes immediately to the left and right of the damageable region as annotated with black circles in Figure 5. The sum of the displacements along the loading direction of these nodes divided by their original distance apart, was used to obtain strain for comparison against test data. It should be noted that the nodes used to determine strain from the FEA are slightly offset from the points used for the virtual extensometer from tests. This was necessary because FEA displacements needed to be extracted from the region outside of the CDM region. Stress was calculated by dividing the applied load by the cross sectional area. The boundary conditions were applied to be consistent with the ASTM standard. Setting the 3-direction displacement, U3, equal to zero in the elastic region was representative of the effect of the compression fixture. The elastic region was composed of continuum shell SC8R elements with a composite shell section definition, and the damageable region was composed of solid C3D8R elements with a solid section definition. Each ply in the damageable region was represented with one layer of C3D8R elements. The separate plies were connected with COH3D8 cohesive elements which were used for modeling delaminations. The approximate mesh size in the damage region was 0.25 mm based on work from [10]. The elastic region was meshed with a free meshing strategy, whereas the damageable region was meshed with a fiber-aligned meshing technique. The fiber-aligned meshing strategy was necessary for implementing the MCS section assignment where only every n^{th} row of elements had matrix damage enabled. Both the DFE and MCS approaches were implemented, with a pattern typical to that shown in Figure 6, where the particular rows of crack-enabled elements were selected such that splitting cracks could occur tangent to the hole. Fiber damage was enabled throughout the CDM region.

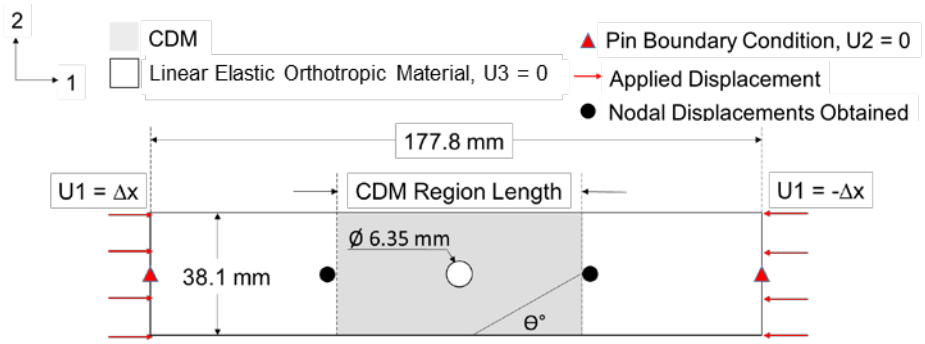

Figure 5. Boundary conditions, section assignments, and geometry for OHC specimen.

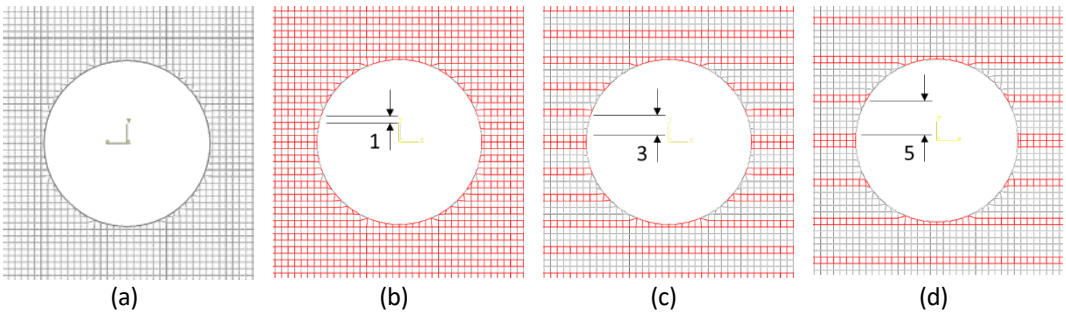

Figure 6. Fiber-aligned mesh for a 0° ply with (a) matrix damage enabled throughout; and with (b) MCS = 1, (c) MCS = 3, and (d) MCS = 5. The regions with matrix damage enabled are highlighted in red for (b), (c), and (d).

Test and Analysis Results

The experimentally measured stress-strain responses are compared to corresponding results from the CDM PDFA results in Figures 7, 8, and 9 for the Delam, Soft and Quasi laminates, respectively. Test and FEA results are shown in red and black, respectively. Red arrows indicate the type of damage initiation for FEA. The order of damage initiation for all FEA were matrix splits, fiber damage, and then delamination. The gray lines represent ±15% from the average experimental strengths and failure strains. The rectangular region created by the gray lines served to provide a visualization of the target strength and failure strain. Analysis results that predicted failure within this envelop were considered to satisfy the success criteria.

The DFE approach (i.e., the model with MCS = 0) consistently under-predicted the target. Test vs. analysis correlation improved with MCS = 1. The analysis predictions for MCS = 3 successfully hit the strength and failure strain targets for both the Delam and Quasi laminates. In the case of the Soft laminate, the test and analysis results for strength were in good agreement. However, the failure strain was under-predicted by the analysis. It should be noted that the analyses were run with linear constitutive response in shear. Introducing a nonlinear shear stress-strain law would likely increase the nonlinearity of the predicted stress vs. strain results and improve the correlation with the failure strain for the Soft laminate. Further increasing the MCS value from 3 to 5 led to analysis predictions overshooting the test results. In general, it was observed that the predicted strength increased with increasing MCS. For still greater values of the MCS, it can be assumed that predicted failure stresses would continue to rise if critical matrix crack locations were missed due to the artificially large distance being placed between matrix cracks.

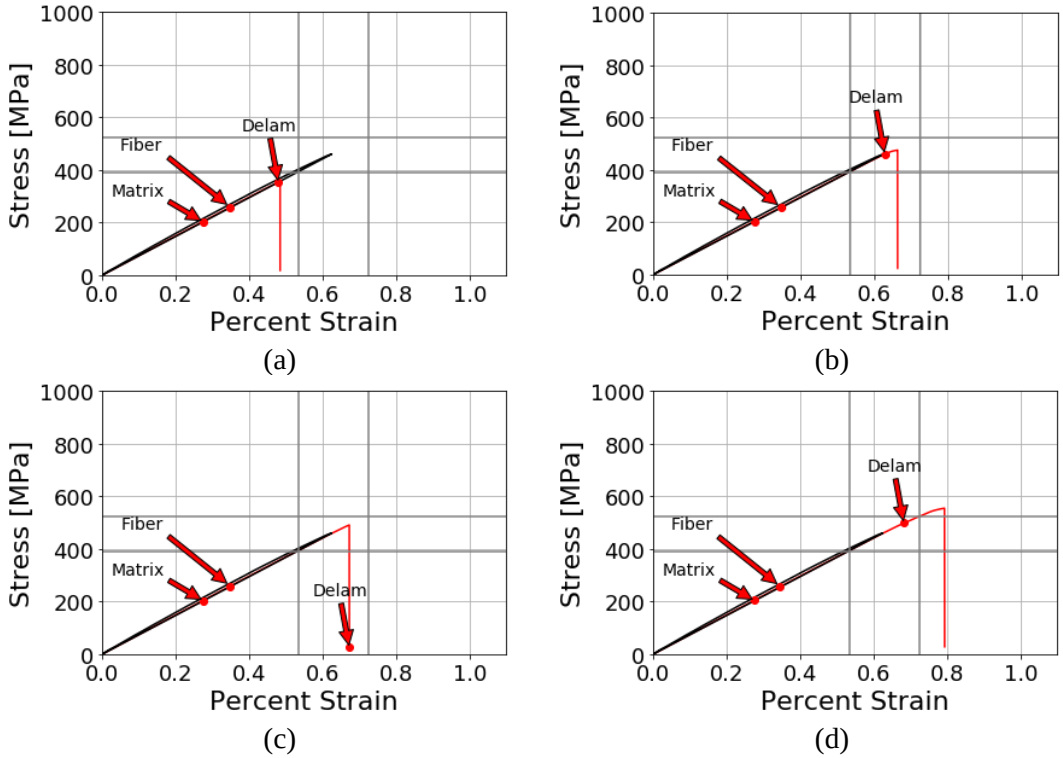

Figure 7. Delam laminate, (a) *DFE or* MCS = 0, (b) MCS = 1, (c) MCS = 3, (d) MCS = 5, where red is FEA, black is test data, gray is ±15% from tests. Damage annotation associated with FEA.

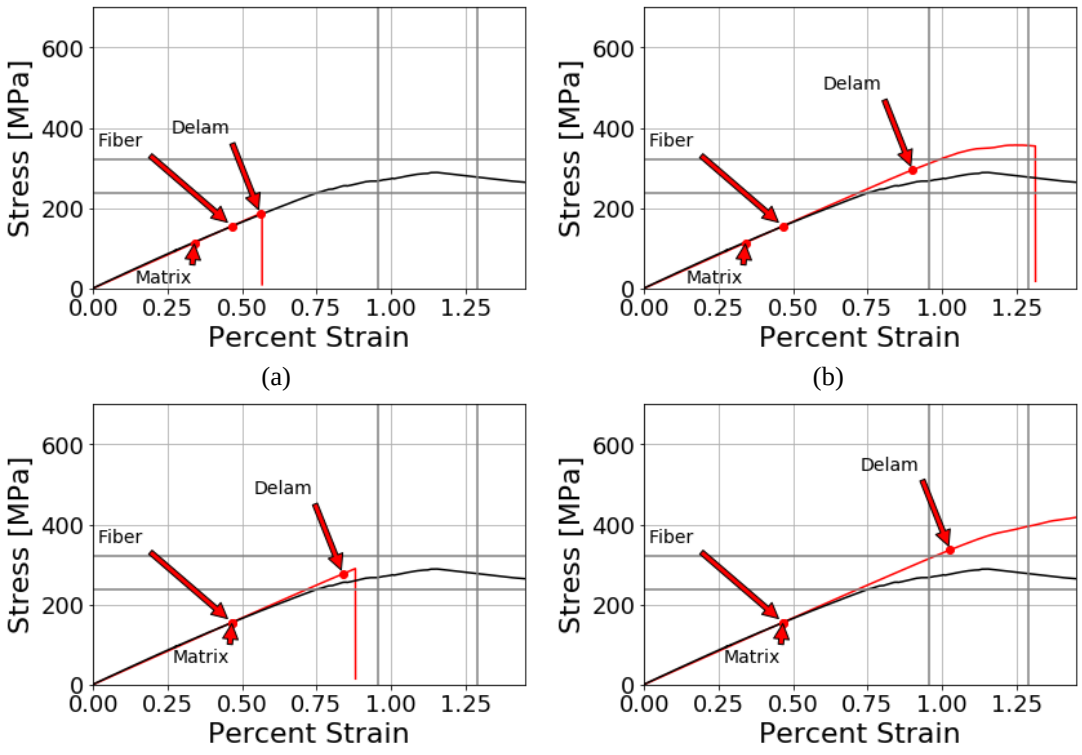

Figure 8. Soft laminate, (a) *DFE or* MCS = 0, (b) MCS = 1, (c) MCS = 3, (d) MCS = 5, where red is FEA, black is test data, gray is ±15% from tests. Damage annotation associated with FEA.

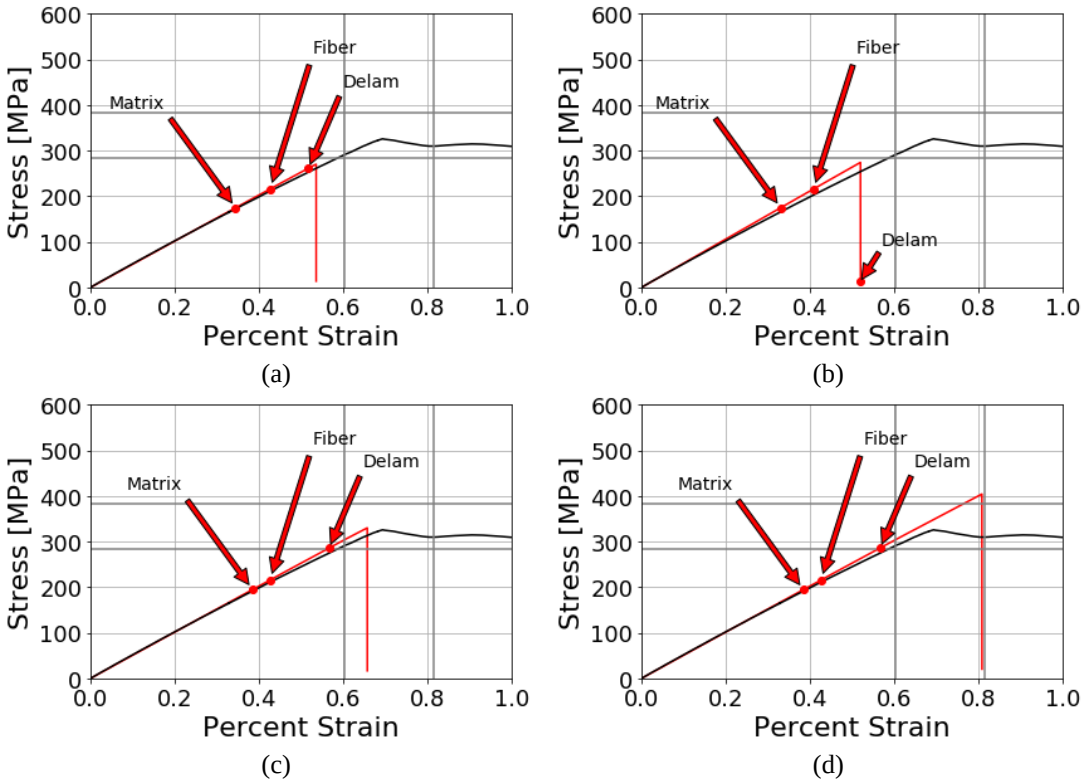

Figure 9. Quasi laminate, (a) *DFE or* MCS = 0, (b) MCS = 1, (c) MCS = 3, (d) MCS = 5, where red is FEA, black is test data, gray is ±15% from tests. Damage annotation associated with FEA.

Since the success criteria were best satisfied when MCS = 3, further investigation into the correlation of the predicted and observed damage process was conducted using the results from these models. Referring to the annotations indicating the onset of matrix and fiber damage in Figures 7–9, it is observed that the analysis results consistently predicted damage significantly prior to the loads at which the tests were interrupted for X-Ray/CT examination. Damage observed in X-ray/CT scans may have developed earlier in the loading than indicated. Damage plots from the models with MCS = 3 were evaluated against existing X-ray CT scans to further understand the correlation between test and analysis results.

The locations of the matrix cracks around the hole are described by the angle β, which is schematically defined in Figure 10. For all displayed X-ray CT data and PDFA comparisons, the loading direction was in the vertical direction, and the 0° fiber direction was along the loading direction. Figures 11–16 illustrate the damage observed from X-ray CT scans and their corresponding CDM matrix damage results. Damage plots obtained from the analyses were extracted for the load levels at which X-ray CT scans were performed in order to provide a one-to-one comparison between X-ray CT data and the analysis predictions. For each laminate, the X-ray CT scans from the specimens loaded to 75% and 90% of the measured strength were used. For CDM damage plots, fully damaged elements are hidden (i.e., damage state variable = 1) and damaged elements are represented in red (i.e., damage state variable < 1).

The experimental and predicted damage states of the OHC Delam specimens loaded to 75% and 90% of ultimate load are shown in Figures 11 and 12, respectively. The central 0° ply group in the OHC test specimen exhibited a large amount of splitting at the edge of the hole on the 75% load level at $\beta = 0°$; however, FEA results showed splitting on both $\beta = 0°$ and $\beta = 180°$. At the 90% load threshold, CT scans revealed significant splitting on both $\beta = 0°$ and $\beta = 180°$. Smaller splits were observed in $\beta = 135°$ and $\beta = 225°$. The analysis results predicted matrix splits at $\beta = 0°$ and $\beta = 180°$, but the predicted matrix damage was not as significant as seen in the X-ray CT scans. The analysis also predicted transverse matrix tension damage at $\beta = 90°$ and $\beta = 270°$. It should be noted that damage shown from X-ray CT scans in Figures 11 and 12 are typical of the red highlighted 0° plies in the captions. Although minute damage was observed in the 45° plies, they are not shown here.

The experimental and predicted damage states for the Soft laminate are shown in Figures 13 and 14 for the 75% and 90% load levels. X-ray CT scans revealed a notable split in the 0° ply near $\beta = 0°$ and a very minor split near $\beta = 180°$, with the crack near $\beta = 0°$ exhibiting a transition from matrix-dominated to fiber-dominated failure. This damage was typical of the 0° plies in this specimen. This damage was observed on both load levels for the test specimens. The analysis predictions show the onset of matrix splitting and fiber compression failure near the matrix splits; but unlike the test specimens, the matrix splits were not fully developed. Similar to the Delam specimens, transverse matrix tension damage was also predicted at $\beta = 90°$, though no evidence of this damage was found in the X-ray CT results.

The Quasi laminate loaded to the 75% load level, exhibited only a small amount of damage in one of the 45° layers at $\beta = 0°$ as shown in Figure 15. At this load level, FEA exhibited a few elements with fully developed damage at $\beta = 45°$ and at $\beta = 225°$. The X-ray CT Scans at the 90% load level contained damage in seven different plies, all of which were 0° and 45° plies, and some of which are shown in Figure 16. The analysis predictions show initiation of matrix splitting at $\beta = 90°$ and $\beta = 270°$ in the 0° plies as

well as additional matrix cracks between these two angles. These additional cracks were not observed in the test specimen at this load level. The analysis also predicted additional crack development in a 45° ply that was also not observed in the tests.

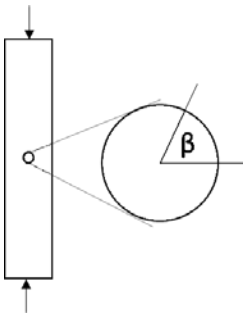

Figure 10. 0° ply orientation and hole loading reference orientation. Damage location around the hole is described by angle β.

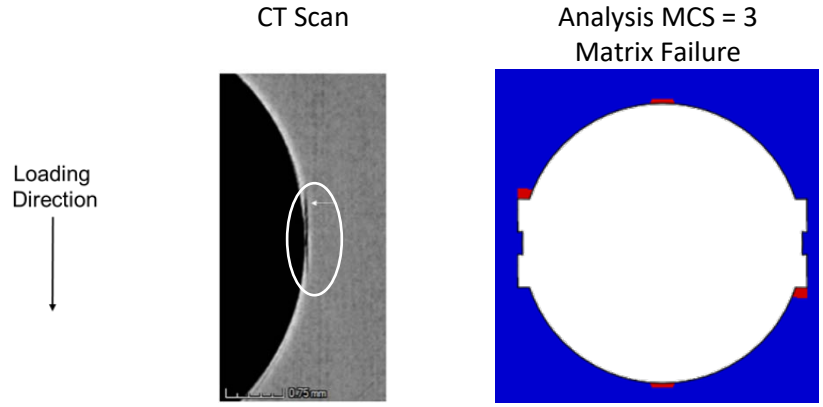

Figure 11. Typical 0° ply matrix splits at 75% of ultimate load for the Delam OHC specimen. Splitting crack (circled in white on CT scan) was observed at β = 0° for the plies shown in red: [+45/−45/0_2/+45/−45/0_2/+45/−45/0_2/0_2/−45/+45/0_2/−45/+45/0_2/−45/+45].

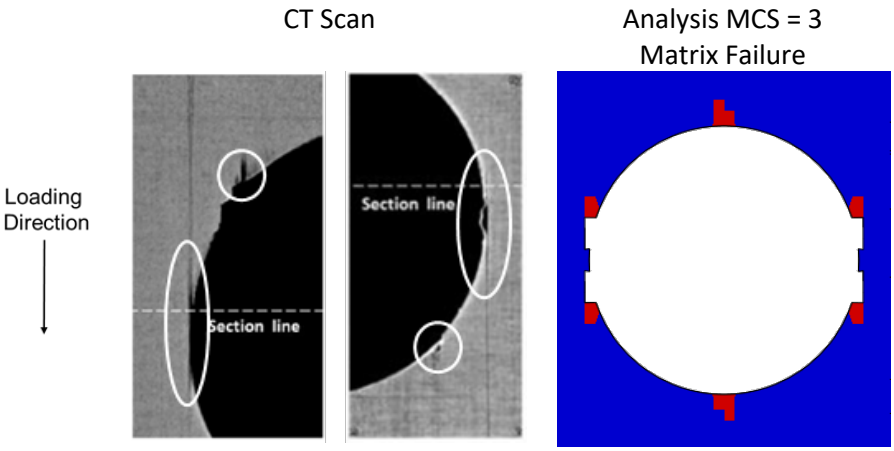

Figure 12. Typical 0° ply matrix splits at 90% of ultimate load for the Delam OHC specimen. Splitting cracks (circled in white on CT scan) were observed on the right hand and left hand side of the hole for the following plies in red: [+45/−45/0_2/+45/−45/0_2/+45/−45/0_2/0_2/−45/+45/0_2/−45/+45/0_2/−45/+45].

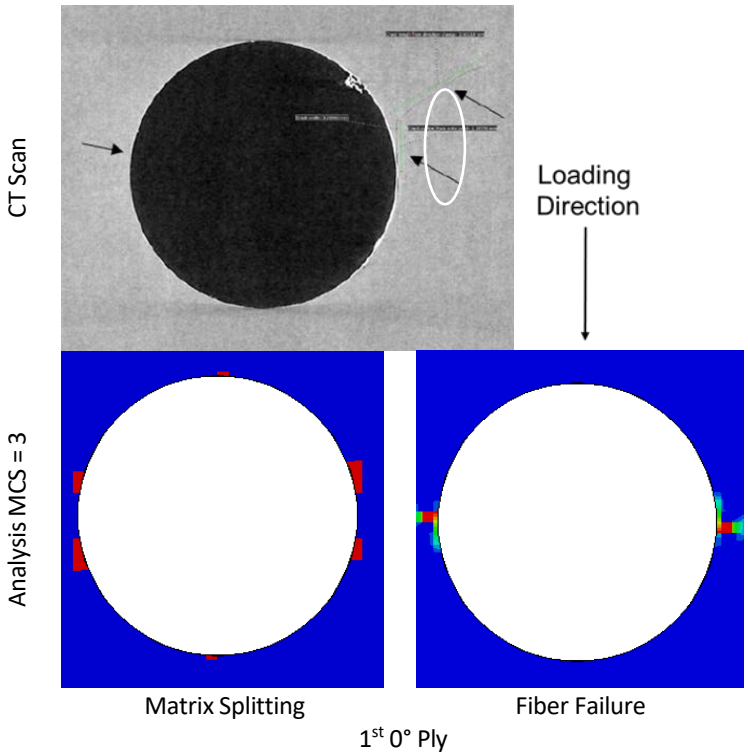

Figure 13. 0° ply matrix splits and fiber failure at 75% of ultimate load for the Soft OHC specimen. Damage observed for the following plies in red: [+45/−45/0/+45/−45/90/+45/−45/+45/−45]s.

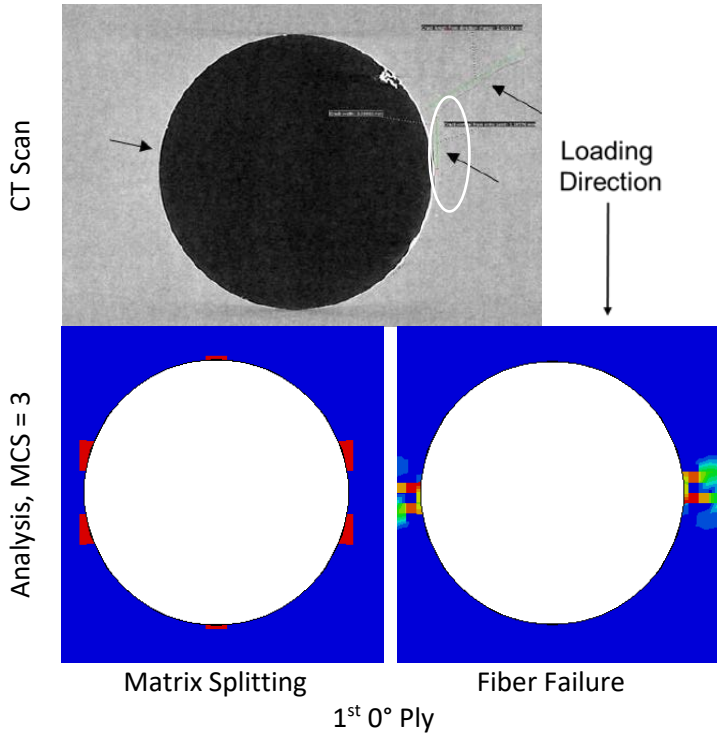

Figure 14. 0° ply matrix splits and fiber failure at 90% of ultimate load for the Soft OHC specimen. Damage observed for the following plies in red: [+45/−45/0/+45/−45/90/+45/−45/+45/−45]s.

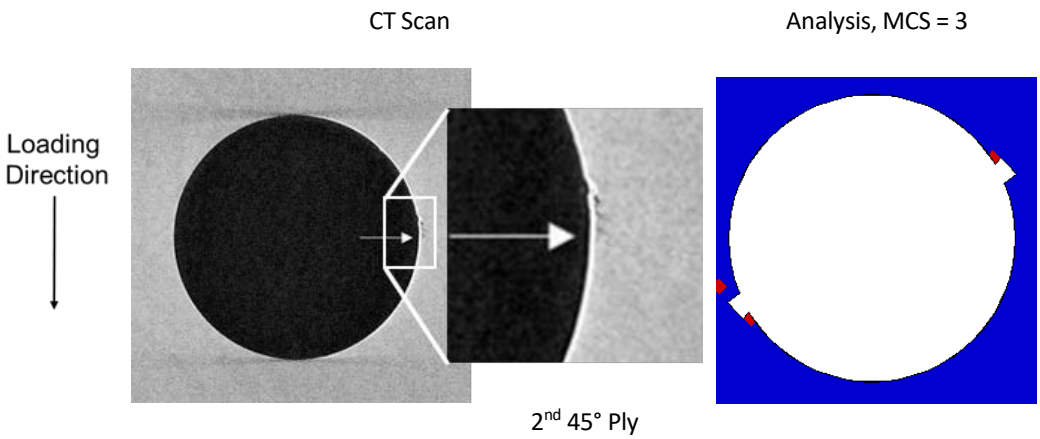

Figure 15. 45° ply matrix splits at 75% of ultimate load for the Quasi OHC specimen. Damage observed for the following plies in red:
[+45/0/−45/90/+45/0/−45/90/+45/0/−45/90/90/−45/0/+45/90/−45/0/+45/90/−45/0/+45].

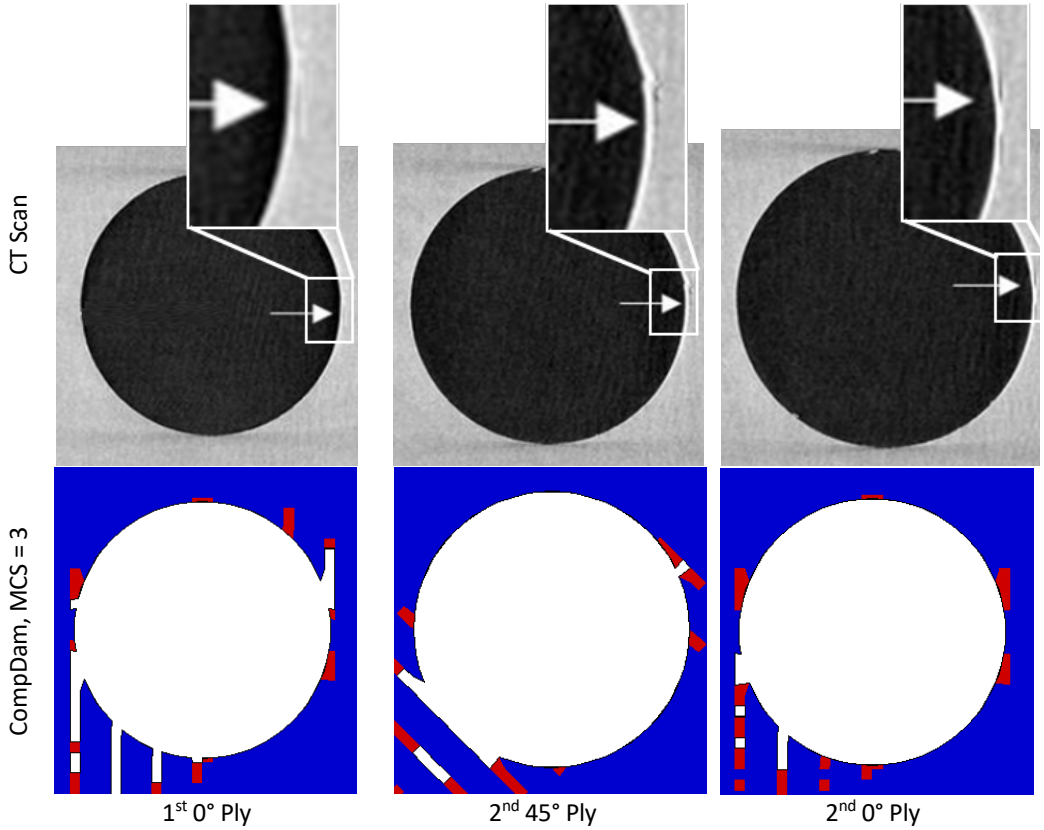

Figure 16. 0° and 45° ply matrix splits at 90% of ultimate load for the Quasi OHC specimen. Damage observed for the plies in red:
[+45/0/−45/90/+45/0/−45/90/+45/0/−45/90/90/−45/0/+45/90/−45/0/+45/90/−45/0/+45].

DISCUSSION

In this study, the effects of augmenting a CDM modeling approach with a matrix crack spacing technique was explored to attempt representing the discrete nature of matrix fracture events. CompDam attempts to represent the kinematics and fracture of

one matrix crack within the height of one element. The mesh and crack density must be selected such that each crack can be treated as an individual crack as opposed to a smeared representation of many cracks. A smeared representation of many cracks, where the analysis predicts regions of parallel cracks, may not necessarily grow or dissipate energy as intended since the stress concentration ahead of the smeared cracks is under-predicted. This study initially explored the MCS approach through a simple unidirectional center notch exercise where the crack spacing was varied. Based on the results shown in Figures 3 and 4, a lower bound for crack spacing, MCS = 3, was determined. The crack spacing approach was then applied to OHC specimens and the results compared with test data in order to validate the analysis approach. Comparisons of stress-strain curves from the test and analysis for four crack spacing values reaffirmed that the lower bound selected from the center notch study was the appropriate MCS value. This is illustrated in Figures 7–9 where the MCS = 3 met the strength and failure strain success criteria.

Reviewing the X-ray CT post-test inspection data revealed that the damage types consisted of splitting in the 0° layer at the edges of the hole and minute damage in the 45° layers. It is important to consider that the compressive loading may induce damage that is not readily observed in the X-ray CT inspection results. The Soft and Quasi laminates included a significant number of 45° plies. The 45° plies provided support to the embedded 0° plies and had a higher compressive strain-to-failure. The 0° ply matrix splits that precede ultimate failure provide strain relief for the stress concentration in the vicinity of the hole; hence a model's ability to capture this event is necessary in order to capture the correct overall failure process. Figures 11–16 showed that although the MCS approach did predict some of the cracks observed in tests, not all of the damage mechanisms were captured. Some additional damage, not observed in the X-ray CT scans, were also predicted.

The differences in analysis predictions and test observations of damage evolution may have been due to the material model assuming a linear constitutive response prior to damage initiation and not including nonlinear stress-strain relationships. Previous work in [10] revealed the need for further refinement of the pre-peak nonlinear model in CompDam and better coupling with compressive damage modes; hence this feature was not used in this study. Oversimplification of the fiber kinking failure mode with a traditional CDM crack-like representation may also contribute to the differences between the test and analysis results. Material models that do not capture both nonlinear and discrete fracture events can produce inaccurate results or may be restricted to use in a design space where nonlinear behavior is minimal. It should also be noted that due to limitations in X-ray CT resolution and difficulty identifying sliding cracks, it is expected that the analysis will predict damage occurs at a lower load level than observation of the corresponding damage in the X-ray CT data. Furthermore, at load levels where subcritical damage propagation has occurred, it seems likely that the analysis will predict damage extends through a larger area than is reported from the X-ray CT data. As such, determination of the uncertainty in the experimental measurements is a necessary step in future validation efforts.

CLOSING REMARKS

This study demonstrates that if a CDM model produces results with adjacent rows of damaged elements, there may not be a sufficient representation of the intact material

between cracks; hence the crack tip stress concentrations become poorly represented and damage predictions suffer. In order to circumvent this issue, a fiber-aligned meshing strategy was used in which only every n^{th} row of elements has matrix damage enabled. Enabling matrix damage in only every n^{th} row can be implemented via a user defined input to represent the spacing between matrix cracks. A lower bound for MCS was obtained by studying the effects of crack front stress development with respect to crack spacing using the CNT and CNS specimens. A potential upper bound for the MCS parameter may be tied to the matrix crack spacing at crack saturation in a given material. When the lower bound for the MCS parameter was used for OHC models, analysis results generally agreed better with validation test data than when damage was fully enabled throughout the areas of interest.

Although model predictions did better agree with experimental results when the matrix crack spacing was imposed, further increases in accuracy are still required, especially for cases where significant nonlinearity occurs prior to collapse. Furthermore, it is necessary to investigate the use of matrix crack spacing techniques with other CDM methods and loading conditions in order to increase confidence in this approach.

ACKNOWLEDGEMENTS

This material is based upon work supported by the National Aeronautics and Space Administration (NASA) under Award No. NNL09AA00A. Any opinions, findings, and conclusions or recommendations expressed in this material are those of the authors and do not necessarily reflect the views of NASA.

REFERENCES

[1] R. D. Young and S. Smeltzer, "Advanced Composites Project," in *CMH-17 PMC Coordination Meeting*, Miami, FL, 2014.

[2] S. P. Engelstad and S. B. Clay, "Comparison of Composite Damage Growth Tools for Static Behavior of Notched Composite Laminates," *Journal of Composite Materials,* vol. 51, no. 10, pp. 1493-1524, 2017.

[3] C. Soutis, A. Fleck and P. A. Smith, "Failure Prediction Technique for Compression Loaded Carbon Fibre-Epoxy Laminate with Open Holes," *Journal of Composite Materials,* vol. 25, no. 11, pp. 1476-1498, 1991.

[4] F. K. Chang and L. B. Lessard, "Damage Tolerance of Laminated Composites Containing an Open Hole and Subjected to Compressive Loadings: Part I - Analysis," *Journal of Composite Materials,* vol. 25, no. 1, pp. 2-43, 1991.

[5] M. Pike, J. D. Schaefer, B. P. Justusson and S. Liguore, "Composite Laminate Progressive Damage Failure Analysis Benchmarking using High Fidelity Inspection Damage Maps," in *AIAA/ASCE/AHS/ASC Structures, Structural Dynamics, and Materials Conference*, AIAA Paper 2018-0734, Kissimmee, FL, 2018.

[6] A. P. K. Joseph, P. Davidson and A. M. Waas, "Failure Analysis of Composite Multi-bolt Joints Using Intra-inter Crack Band Model (I2CBM)," in *AIAA/ASCE/AHS/ASC Structures, Structural Dynamics, and Materials Conference,* AIAA Paper 2018-0977, Kissimmee, FL, 2018.

[7] F. A. Leone, "Deformation Gradient Tensor Decomposition for Representing Matrix Cracks in Fiber-Reinforced Composite Structures," *Composites Part A: Applied Science and Manufacturing,* vol. 76, pp. 334-341, 2015.

[8] F. A. Leone and A. Bergan, "CompDam_DGD Version 1.0.1," GitHub repository, [Online]. Available: https://github.com/nasa/CompDam_DGD.

[9] S. Wanthal, J. Schaefer, B. Justusson, I. Hyder, S. Engelstad and C. Rose, "Verification and Validation Process for Progressive Damage and Failure Analysis Methods in the NASA Advanced Composites Consortium," in *American Society for Composites Technical Conference*, West Lafayette, IN, 2017.

[10] I. Hyder, J. Schaefer, B. Justusson, S. Wanthal, F. Leone and C. Rose, "Assesment of Intralaminar Progressive Damage and Failure Analysis Methods Using an Efficient Evaluation Framework," in *American Society for Composites Technical Conference*, West Lafayette, IN, 2017.

[11] F. A. Leone, C. G. Davila, G. E. Mabson, M. Ramnath and I. Hyder, "Fracture-Based Mesh Size Requirements for Matrix Cracks in Continuum Damage Mechanics Models," in *AIAA/ASCE/AHS/ASC Structures, Structural Dynamics, and Materials Conference*, AIAA Paper 2017-0198, Grapevine, TX, 2017.

[12] American Society for Testing Materials, "ASTM D6484, Standard Test Method for Open Hole Compressive Strength of Polymer Matrix Composite Laminates," Philadelphia, PA, 2006.

[13] S. Wanthal, B. Justusson, J. Schaefer, I. Hyder, M. Pike, B. Owen, H. Gu, S. Engelstad, A. Selvarathinam, R. Stover, J. Action, B. Cranston, C. Rose, T. K. O'Brien, C. Davila, F. Leone, A. Bergan, W. Jackson, W. Johnston and K. Song, "PDA Blind Prediction Analysis Report, 2C14 - Post-Buckled Panel with BVID, Strength and Life," Advanced Composite Consortium Cooperative Agreement NNL09AA00A, 2017.